ESO-Based Model-Free Adaptive Heading Control for Unmanned Surface Vessels

Shuaixi Li, Yongchao Liu, and Ge Song

***Abstract*—A model-free adaptive heading control strategy for unmanned surface vessels (USVs) is proposed by integrating extended state observer (ESO) with model-free adaptive control. To handle internal model perturbations and external disturbances, a discrete linear ESO is employed to estimate the aggregate uncertainties. Then, the model-free adaptive heading controller is constructed by utilizing system input and output data, and the estimation information deriving from the ESO. Furthermore, a dynamic event-triggered mechanism (ETM) is designed and embedded in the controller to save communication data. Compared with the periodic sampling, the introduction of the dynamic ETM enables the controller to achieve a comparable control performance with only 5.35% of the communication frequency. Simulation comparison and analysis exhibit that the proposed heading controller can achieve superior heading control effect for USVs and show broader application prospect.**

***Index Terms*—Heading control, extended state observer (ESO), dynamic event-triggered control, unmanned surface vessels (USVs)**

I. Introduction

UNMANNED surface vessels (USVs) have become indispensable platforms for a wide range of maritime missions [1]. Their applications encompass oceanographic mapping and environmental monitoring, maritime search and rescue, port security and surveillance, and even military operations [2–4]. The autonomous execution of these tasks in complex and dynamic marine environments imposes stringent requirements on reliable and precise motion control systems. Among these, heading control is the most critical and fundamental component in the USV motion control [5, 6].

Despite its significance, it is a substantial challenge to achieve high-performance heading control for USVs. The nonlinear and coupled dynamics of USVs are susceptible to model disturbances because of changes in payload, mass, and inertia. In addition, USVs are continuously subjected to unmeasurable and time-varying disturbances such as wind, waves, and ocean currents. These factors collectively form a lumped disturbance that can severely degrade control performance, leading to steady-state error and excessive overshoot.

To address these challenges, great efforts have been devoted to USV heading control, with lots of significative achievements being discovered [7–10]. In Ref. [7], an adaptive dynamic surface control scheme is proposed by combining backstepping technology and Nussbaum gain function, which can ensure that the heading angle converges and remains at its preset value even when the control coefficients are unknown. In Ref. [8], a neural adaptive steering control design is proposed to address measurement noise and unknown dynamics while avoiding the amplification of noise caused by the first-order filters. In Ref. [9], a global finite-time heading control scheme is developed that can ensure the heading angle converges to its desired value within a bounded time interval. To address the issues of input saturation and environment disturbances, a robust heading adaptive controller is designed by introducing auxiliary dynamics system and Nussbaum function [10]. However, these methods often depend on an accurate mathematical representation of the yaw dynamics. It is difficult to get accurate model information because of the external disturbances and internal uncertainties.

The limitations of model dependency have spurred growing interest in data-driven control approaches. Model-free adaptive control (MFAC) is a method that directly generates control signals from the input-output data of the system [11–13]. By utilizing a dynamic linearization technique to construct a virtual linear data model online, MFAC achieves satisfactory control performance using only the input-output data for complex nonlinear systems. However, when the standard MFAC framework is applied directly to USV heading control, it often results in sluggish responses or oscillations because of the non-self-stabilizing characteristic of yaw dynamics. Liao et al. [14] proposed a redefined-output MFAC (RO-MFAC) method for USV heading control by introducing a redefined output gain. To address the sensitivity issue associated with the redefined output gain, a control output constraint function is incorporated into the RO-MFAC scheme [15]. In Ref. [16], a variable-output MFAC method is proposed by integrating historical input signals into the standard control criterion function, thereby weakening the integral action within the system of heading control.

Furthermore, the above strategies are based on the periodic sampling, which leads to excessive and unnecessary signal communication and computational burdens in practical applications. Event-triggered control (ETC) is a practical approach

Manuscript received: 4 September 2025; revised: 22 September 2025; accepted: 28 September 2025. *(Corresponding author: Yongchao Liu.)*

Citation: S. Li, Y. Liu, and G. Song, ESO-based model-free adaptive heading control for unmanned surface vessels, *Int. J. Intell. Control Syst.*, 2025, 30(4), 307–313.

Shuaixi Li and Yongchao Liu are with School of Automation, Qingdao University, Qingdao 266071, China (e-mail: 2018205638@qdu.edu.cn; sdliuyc@qdu.edu.cn).

Ge Song was with Institute for Aerospace Studies, University of Toronto, Toronto M3H 5T6, Canada, and is now with School of Automation, Harbin University of Science and Technology, Harbin 150080, China (e-mail: gesong@mail.utoronto.ca).

Digital Object Identifier 10.62678/IJICS202512.10232

for conserving network resources and reducing communication frequency [17–19]. The event-triggered mechanism (ETM) is applied to the communication channel, with the core idea being that data transmission and control updates are executed only when a pre-defined triggering condition is satisfied. An event-triggered MFAC is introduced with a static ETM [20]. In Ref. [21], a dynamic event-triggered MFAC is developed to further lower network transmission frequency. A data-driven resilient heading control method is proposed by combining dynamic event-triggering and neural networks [22], which also represents an extension of the RO-MFAC scheme. In Ref. [23], an adaptive fuzzy heading control strategy is developed by combining input quantization and ETM, which uses a fuzzy logic system to handle external disturbances and model uncertainties.

To simultaneously address the issues of lumped disturbance and the non-self-stabilizing characteristic in the heading control system, this paper proposes a model-free adaptive heading control (MFAHC) strategy that combines extended state observer (ESO) and dynamic ETM. The major contributions can be outlined as follows:

(1) The output of the MFAC is redefined by incorporating angular velocity alongside the heading angle. Therefore, the proposed MFAHC strategy has critical damping characteristic, which can address the under-damped and non-self-stabilizing characteristics of USV heading dynamics.

(2) A discrete linear ESO is designed and embedded into the control loop to actively estimate the lumped disturbance, comprising both internal model uncertainty and external environmental disturbances. Then, the estimation is fed into the MFAC law for compensation, which can enhance the system's robustness and reduce oscillation amplitude. Therefore, the proposed ESO-based MFAHC strategy can achieve superior heading convergence performance in the presence of lumped disturbance.

(3) A dynamic ETM is designed in the control framework. The mechanism utilizes an internal dynamic variable coupled with the sampling error, which can ensure the efficient use of communication bandwidth and computational resources by reducing unnecessary updates during steady-state operation. Therefore, the proposed MFAHC strategy with dynamic ETM can maintain better convergence performance even after a significant reduction in communication frequency.

II. PROBLEM STATEMENT

Consider a discrete-time heading control system [1]

$$\begin{cases} \psi(k+1) = \psi(k) + T_{\mathrm{s}} \cdot r(k), \\ r(k+1) = r(k) + T_{\mathrm{s}} \cdot \dfrac{K\delta(k) - r(k) + d(k)}{T} \end{cases} \tag{1}$$

where T_{s} denotes the sampling interval, and K and T are model parameters. The variables $r(k)$ and $\psi(k)$ are angular velocity and heading angle, respectively. $\delta(k)$ is the rudder angle and $d(k)$ denotes the ocean disturbance.

According to $\Delta\psi(k) = \psi(k) - \psi(k-1)$, $\Delta\psi(k+1) = \psi(k+1) - \psi(k)$, etc., Eq. (1) can be expressed in the incremental form

$$\begin{cases} \Delta\psi(k+1) = \Delta\psi(k) + T_{\mathrm{s}} \cdot \Delta r(k), \\ \Delta r(k+1) = \Delta r(k) + T_{\mathrm{s}} \cdot \dfrac{K\Delta\delta(k) - \Delta r(k) + \Delta d(k)}{T} \end{cases} \tag{2}$$

Redefine the system output in the following form

$$y(k+1) = \psi(k+1) + cr(k+1) \tag{3}$$

where $c > 0$ is a gain parameter. The angular velocity is incorporated via c to form a composite system output with the heading angle. Such operation can make the system satisfy the assumptions of MFAC and solve the non-self-balancing problem of the second-order heading control system.

Substitute Eq. (3) into Eq. (2) to obtain the following redefined system

$$\begin{aligned} \Delta y(k+1) = \Delta\psi(k+1) + c\Delta r(k+1) = \\ \Delta\psi(k) + T_{\mathrm{s}} \cdot \Delta r(k) + c\Delta r(k) + \\ \frac{T_{\mathrm{s}} c}{T} \cdot [K\Delta\delta(k) - \Delta r(k) + \Delta d(k)] \end{aligned} \tag{4}$$

Letting $\omega(k) = \Delta\psi(k) + (T_{\mathrm{s}} + c)\Delta r(k) + T_{\mathrm{s}} c/T \cdot [\Delta d(k) - \Delta r(k)]$ and $\phi(k) = T_{\mathrm{s}} cK/T$, Eq. (4) can be transformed as

$$\Delta y(k+1) = \phi(k)\Delta\delta(k) + \omega(k) \tag{5}$$

where $\omega(k)$ is the lumped disturbance term and $\phi(k)$ is the partial derivative of Eq. (4) with $\Delta\delta(k)$.

III. CONTROLLER DESIGN AND STABILITY ANALYSIS

Fig. 1 shows a schematic diagram of the proposed model-free adaptive heading control strategy. It includes the estimator of $\phi(k)$, the discrete linear ESO, the dynamic ETM, the redefined-output module, and the heading controller.

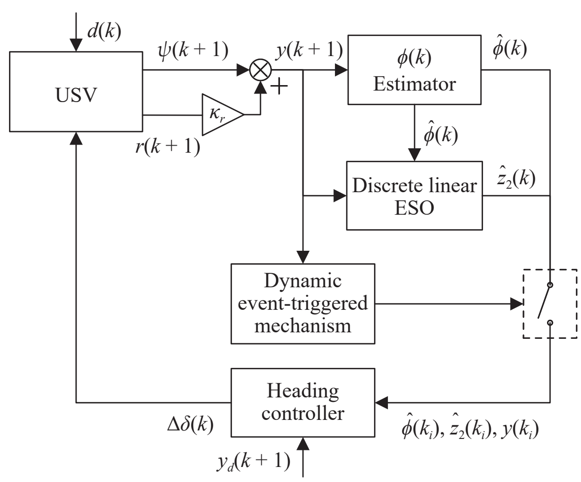

Fig. 1 Framework of ESO-based MFAHC strategy.

A. Controller Design

Assumption 1 The ocean disturbance $d(k)$ and its variation $\Delta d(k)$ are bounded, i.e., $d(k) \leqslant b_d$ and $\Delta d(k) \leqslant b_{\Delta,d}$.

Assumption 2 Equation (4) possesses generalized Lipschitz continuity, as $\forall k_1 \neq k_2$, where $k_1, k_2 \geqslant 0$ and $\delta(k_1) \neq \delta(k_2)$, then $|y(k_1+1) - y(k_2+1)| \leqslant b_1 |\delta(k_1) - \delta(k_2)|$, where $b_1 > 0$ is a constant.

Assumption 3 The partial derivative of Eq. (4) with respect to the control input $\Delta\delta(k)$ exists and its sign keep invariant, i.e., $\phi(k) < 0$ or $\phi(k) > 0$.

Remark 1 Since K and T are positive parameters, it implies that the $\phi(k)$ defined in Eq. (5) satisfies Assumption 3.

Since $\phi(k)$ is unknown, an estimation algorithm is designed as

$$\hat{\phi}(k)=\hat{\phi}(k-1)+\frac{\eta\Delta\delta(k-1)}{\mu+\Delta\delta(k-1)^2}\cdot[\Delta y(k)-\hat{\phi}(k-1)\Delta\delta(k-1)] \tag{6}$$

$$\hat{\phi}(k)=\hat{\phi}(0),\quad \text{if}\left|\hat{\phi}(k)\right|\leqslant\varepsilon \quad\text{or}\quad |\Delta\delta(k-1)|\leqslant\varepsilon \quad\text{or}\quad \text{sign}(\hat{\phi}(k))\neq\text{sign}(\hat{\phi}(0)) \tag{7}$$

where $\eta\in(0,1]$ is used to optimize the estimation algorithm, ε is a positive small constant, and $\mu>0$ is used to limit the rate of change of $\hat{\phi}(k)$. Formula (7) is a reset mechanism for the estimation algorithm.

Define $z_1(k)=y(k)$ and $z_2(k)=\omega(k)$. From Eq. (5), we can get

$$\begin{cases}z_1(k+1)=z_1(k)+\phi(k)\Delta\delta(k)+z_2(k),\\ z_2(k+1)=z_2(k)+\omega(k+1)-\omega(k)\end{cases} \tag{8}$$

Then, design the following discrete linear ESO

$$\begin{cases}\hat{z}_1(k+1)=\hat{z}_1(k)+\hat{\phi}(k)\Delta\delta(k)+\hat{z}_2(k)+l_1\tilde{z}_1(k),\\ \hat{z}_2(k+1)=\hat{z}_2(k)+l_2\tilde{z}_1(k)\end{cases} \tag{9}$$

where $\tilde{z}_1(k)=z_1(k)-\hat{z}_1(k)$, $\hat{z}_1(k)$ and $\hat{z}_2(k)$ represent the estimate values of $z_1(k)$ and $z_2(k)$, respectively, and l_1 and l_2 are the gain parameters to be designed.

Define a performance function as

$$J[\delta(k)]=[y_d(k+1)-y(k)-\phi(k)\Delta\delta(k)-z_2(k)]^2+\lambda[\delta(k)-\delta(k-1)]^2 \tag{10}$$

where $y_d(k+1)$ is a reference signal, and $\lambda>0$ is a parameter to prevent $\Delta\delta(k)$ from becoming too large. By taking the partial derivative of Eq. (10) concerning $\delta(k)$ and solving for the extreme points, we construct the following ideal control algorithm

$$\delta(k)=\delta(k-1)+\frac{\gamma\phi(k)}{\lambda+\phi(k)^2}[y_d(k+1)-y(k)-z_2(k)] \tag{11}$$

where $\gamma\in(0,1]$ is used to optimize the control algorithm.

To save communication resources, the condition of a dynamic ETM is formulated as

$$k_{i+1}=\inf\{k\in\mathbb{N}\mid k>k_i, g(k)<0\} \tag{12}$$

where $g(k)=|h(k)|/\vartheta+\varpi-|m(k)|$, $\vartheta>0$ and $\varpi>0$ are design parameters, $m(k)=y(k)-y(k_i)$ represents the sampling error, and $\{k_i,\ i=0,1,\ldots\}$ is the set consisting of all the event-triggered moments. The dynamic variable $h(k)$ is updated as

$$h(k+1)=\varphi h(k)+\varpi-|m(k)| \tag{13}$$

where $\varphi>0$ is a design parameter and $h(0)=h_0$ is the initial value of $h(k)$.

Combining estimation algorithm in Eq. (6), discrete linear ESO in Eq. (9), and dynamic ETM in Eq. (12), we substitute $\hat{\phi}(k_i)$ and $\hat{z}_2(k_i)$ into Eq. (11) to obtain

$$\delta(k)=\delta(k-1)+\frac{\gamma\hat{\phi}(k_i)}{\lambda+\hat{\phi}(k_i)^2}[y_d(k+1)-y(k_i)-\hat{z}_2(k_i)] \tag{14}$$

B. Stability Analysis

Lemma 1 [24] Consider a discrete-time linear system

$$\boldsymbol{x}(k+1)=\boldsymbol{A}\boldsymbol{x}(k)+\boldsymbol{B}\boldsymbol{u}(k) \tag{15}$$

where $\boldsymbol{x}\in\mathbb{R}^n$ is the state, and $\boldsymbol{u}\in\mathbb{R}^m$ is the input. For the given matrices $\boldsymbol{A}\in\mathbb{R}^{n\times n}$ and $\boldsymbol{B}\in\mathbb{R}^{n\times m}$, if the spectral radius of $\boldsymbol{A}$ satisfies $\rho(\boldsymbol{A})<1$ and $\boldsymbol{B}\boldsymbol{u}(k)$ is bounded, then the system state $\boldsymbol{x}(k)$ is bounded.

Assumption 4 The bounded control input signal $\delta(k)$ can always be found to drive the system output $y(k+1)$ to $y_d(k+1)$, where $y_d(k+1)$ is a bounded reference signal.

Assumption 5 The desired heading angle $\psi_d(k)$ and desired angular velocity $r_d(k)$ are bounded and their increments are bounded, i.e., $|y_d(k)|=\left|\psi_d(k)+cr_d(k)\right|\leqslant b_{\Delta,y}$, where $b_{\Delta,y}>0$ is a constant.

Theorem 1 Under Assumptions 1–3, the estimation algorithm in Eq. (6) and reset mechanism in Formula (7) can ensure that the estimation error $\tilde{\phi}(k)=\hat{\phi}(k)-\phi(k)$ is uniformly ultimately bounded (UUB) by selecting parameters $\mu>0$ and $\eta\in(0,1]$.

Proof When the reset mechanism in Formula (7) is satisfied, $\hat{\phi}$ is clearly bounded. In other cases, it follows from Eqs. (5) and (6) that

$$\begin{aligned}\tilde{\phi}(k)=\;&\hat{\phi}(k)-\phi(k-1)+\phi(k-1)-\phi(k)=\\ &\hat{\phi}(k-1)-\phi(k-1)+\frac{\eta\Delta\delta(k-1)}{\mu+\Delta\delta(k-1)^2}\cdot\\ &[\Delta y(k)-\hat{\phi}(k-1)\Delta\delta(k-1)]+\phi(k-1)-\phi(k)=\\ &\tilde{\phi}(k-1)+\frac{\eta\Delta\delta(k-1)^2}{\mu+\Delta\delta(k-1)^2}[\phi(k-1)-\hat{\phi}(k-1)]+\\ &\frac{\eta\Delta\delta(k-1)\omega(k-1)}{\mu+\Delta\delta(k-1)^2}+\phi(k-1)-\phi(k)=\\ &\left[1-\frac{\eta\Delta\delta(k-1)^2}{\mu+\Delta\delta(k-1)^2}\right]\tilde{\phi}(k-1)+\\ &\frac{\eta\Delta\delta(k-1)}{\mu+\Delta\delta(k-1)^2}\omega(k-1)+\phi(k-1)-\phi(k)\end{aligned} \tag{16}$$

By taking the absolute value of Eq. (16), we obtain

$$\begin{aligned}|\tilde{\phi}(k)|\leqslant\;&\left|1-\frac{\eta\Delta\delta(k-1)^2}{\mu+\Delta\delta(k-1)^2}\right||\tilde{\phi}(k-1)|+\\ &\left|\frac{\eta\Delta\delta(k-1)}{\mu+\Delta\delta(k-1)^2}\right||\omega(k-1)|+\\ &|\phi(k-1)-\phi(k)|\end{aligned} \tag{17}$$

where $\dfrac{\eta\Delta\delta(k-1)^2}{\mu+\Delta\delta(k-1)^2}$ is regarded as a monotone increasing function of $\Delta\delta(k-1)^2$. By combining the reset mechanism in Formula (7), we have

$$\frac{\eta\Delta\delta(k-1)^2}{\mu+\Delta\delta(k-1)^2}\geqslant\frac{\eta\varepsilon^2}{\mu+\varepsilon^2} \tag{18}$$

where $0<\eta\leqslant 1$ and $\mu>0$. We can find a constant g_1 that makes

$$0\leqslant\left|1-\frac{\eta\Delta\delta(k-1)}{\mu+\Delta\delta(k-1)^2}\right|\leqslant 1-\frac{\eta\varepsilon^2}{\mu+\varepsilon^2}\triangleq g_1<1 \tag{19}$$

and

$$\left|\frac{\eta\Delta\delta(k-1)}{\mu+\Delta\delta(k-1)^2}\right|\leqslant\frac{\eta|\Delta\delta(k-1)|}{2\sqrt{\mu}|\Delta\delta(k-1)|}\leqslant\frac{\eta}{2\sqrt{\mu}} \tag{20}$$

According to Assumption 2 and the definition of $\phi(k)$, $\phi(k)$ is bounded, satisfying $|\phi(k)| \leqslant b_\phi$ and $|\phi(k-1)-\phi(k)| \leqslant 2b_\phi$. According to Assumption 1 and the definition of $\omega(k)$, $\omega(k)$ is bounded, satisfying $|\omega(k)| \leqslant b_\omega$. Then, combining with Formulas (19) and (20), we obtain

$$\begin{aligned}|\tilde{\phi}(k)| &\leqslant g_1|\tilde{\phi}(k-1)| + \frac{\eta b_\omega}{2\sqrt{\mu}} + 2b_\phi \leqslant \\ & g_1^2|\tilde{\phi}(k-2)| + g_1\left(\frac{\eta b_\omega}{2\sqrt{\mu}} + 2b_\phi\right) + \frac{\eta b_\omega}{2\sqrt{\mu}} + 2b_\phi \leqslant \\ & \cdots \leqslant g_1^{k-1}|\tilde{\phi}(1)| + \frac{b_1(1-g_1^{k-1})}{1-g_1}\end{aligned} \tag{21}$$

where $b_1 = \dfrac{\eta b_\omega}{2\sqrt{\mu}} + 2b_\phi$. When $k \to \infty$, $\dfrac{b_1(1-g_1^{k-1})}{1-g_1} = \dfrac{b_1}{1-g_1}$. This means that $\tilde{\phi}(k)$ is UUB, and we obtain that $\hat{\phi}(k)$ is bounded under the boundedness of $\phi(k)$. ■

Theorem 2 Under Assumptions 1–3, the discrete linear ESO in Eq. (9) can ensure that the state estimation errors $\tilde{z}_1(k) = z_1(k) - \hat{z}_1(k)$ and $\tilde{z}_2(k) = z_2(k) - \hat{z}_2(k)$ are bounded by selecting parameters l_1 and l_2 that satisfy

$$\max\left\{\left|\frac{-\sqrt{l_1^2-4l_2}+2-l_1}{2}\right|, \left|\frac{\sqrt{l_1^2-4l_2}+2-l_1}{2}\right|\right\} < 1 \tag{22}$$

Proof Equation (8) can be rewritten as the following vector form

$$z(k+1) = \boldsymbol{A}z(k) + \boldsymbol{B}(k)\Delta\delta(k) + \boldsymbol{D}[\omega(k+1)-\omega(k)] \tag{23}$$

where $z(k) = [z_1(k), z_2(k)]^{\mathrm{T}}$, $\boldsymbol{B}(k) = [\phi(k), 0]^{\mathrm{T}}$, $\boldsymbol{D} = [0,1]^{\mathrm{T}}$, and

$$\boldsymbol{A} = \begin{bmatrix}1 & 1\\ 0 & 1\end{bmatrix} \tag{24}$$

The discrete linear ESO in Eq. (9) can be represented in vector form as

$$\hat{z}(k+1) = \boldsymbol{A}\hat{z}(k) + \hat{\boldsymbol{B}}(k)\Delta\delta(k) + \boldsymbol{LC}[z(k+1) - \hat{z}(k)] \tag{25}$$

where $\hat{z}(k) = [\hat{z}_1(k), \hat{z}_2(k)]^{\mathrm{T}}$, $\hat{\boldsymbol{B}}(k) = [\hat{\phi}(k), 0]^{\mathrm{T}}$, $\boldsymbol{L} = [l_1, l_2]^{\mathrm{T}}$, and $\boldsymbol{C} = [1, 0]$.

Defining the state estimation error vector as $\tilde{z}(k) = z(k) - \hat{z}(k)$, we obtain

$$\begin{aligned}\tilde{z}(k+1) = z(k+1) - \hat{z}(k+1) = & \\ & \boldsymbol{A}\tilde{z}(k) - \boldsymbol{LC}\tilde{z}(k) + \boldsymbol{B}(k)\Delta\delta(k) - \hat{\boldsymbol{B}}(k)\Delta\delta(k) + \\ & \boldsymbol{D}[\omega(k+1)-\omega(k)] = \\ & (\boldsymbol{A}-\boldsymbol{LC})\tilde{z}(k) + \tilde{\boldsymbol{B}}(k)\Delta\delta(k) + \\ & \boldsymbol{D}[\omega(k+1)-\omega(k)]\end{aligned} \tag{26}$$

where $\tilde{\boldsymbol{B}}(k) = [-\tilde{\phi}(k), 0]^{\mathrm{T}}$. For the actual heading control system, the change in rudder angle is limited, so $\Delta\delta(k)$ is bounded. According to Theorem 1, $\tilde{\phi}(k)$ and $\omega(k)$ are bounded. We select appropriate parameters l_1 and l_2 to ensure that the spectral radius of $\boldsymbol{A}-\boldsymbol{LC}$ satisfies $\rho(\boldsymbol{A}-\boldsymbol{LC}) < 1$, that is

$$\begin{aligned}&\rho(\boldsymbol{A}-\boldsymbol{LC}) = \\ &\max\left\{\left|\frac{2-l_1+\sqrt{l_1^2-4l_2}}{2}\right|, \left|\frac{2-l_1-\sqrt{l_1^2-4l_2}}{2}\right|\right\} < 1\end{aligned} \tag{27}$$

According to Lemma 1, $\rho(\boldsymbol{A}-\boldsymbol{LC}) < 1$ and the term $\tilde{\boldsymbol{B}}(k)\Delta\delta(k) + \boldsymbol{D}[\omega(k+1)-\omega(k)]$ in the error dynamics Eq. (26) can be viewed as a bounded input. It then follows that $\tilde{z}(k)$ is bounded and consequently $\hat{z}(k)$ is also bounded for the bounded $\omega(k)$. ■

Theorem 3 Under Assumptions 1–5, the control algorithm in Eq. (14) can ensure that the tracking error $\tilde{e}(k) = y_d(k) - y(k)$ is UUB by selecting parameters $0 < \varphi + 1/\vartheta < 1$, $\varpi > 0$, $\gamma \in (0,1]$, and $\lambda > \lambda_{\min}$, where $\lambda_{\min} = b_\phi^2/4$.

Proof According to the event-triggered condition in Eq. (12), it can be obtained that $g(k) = |h(k)|/\vartheta + \varpi - |m(k)| \geqslant 0$ at $k \in [k_i, k_{i+1})$. The dynamic variable $h(k)$ satisfies

$$\begin{aligned}|h(k+1)| &\leqslant \varphi|h(k)| + \varpi + |m(k)| \leqslant \\ & \varphi|h(k)| + \varpi + \frac{1}{\vartheta}|h(k)| + \varpi \leqslant \\ & \left(\varphi + \frac{1}{\vartheta}\right)|h(k)| + 2\varpi \leqslant \\ & \left(\varphi + \frac{1}{\vartheta}\right)^2|h(k-1)| + 2\left(\varphi + \frac{1}{\vartheta}\right)\varpi + 2\varpi \leqslant \\ & \cdots \leqslant \left(\varphi + \frac{1}{\vartheta}\right)^k|h(1)| + \frac{2\varpi\left[1-\left(\varphi+\frac{1}{\vartheta}\right)^k\right]}{1-\left(\varphi+\frac{1}{\vartheta}\right)}\end{aligned} \tag{28}$$

Select the appropriate parameters to ensure that $0 < \varphi + 1/\vartheta < 1$. When $k \to \infty$, we can get $\dfrac{2\varpi\left[1-\left(\varphi+\frac{1}{\vartheta}\right)^k\right]}{1-\left(\varphi+\frac{1}{\vartheta}\right)} = \dfrac{2\varpi}{1-\left(\varphi+\frac{1}{\vartheta}\right)}$. This means that $h(k)$ is UUB.

Next, according to Eqs. (5) and (14) at $k \in [k_i, k_{i+1})$, we have

$$\begin{aligned}\tilde{y}(k+1) = y_d(k+1) - y(k+1) = & \\ & y_d(k+1) - y_d(k) + y_d(k) - y(k) - \\ & \phi(k)\Delta\delta(k) - \omega(k) = \\ & \Delta y_d(k+1) + \tilde{y}(k) - \omega(k) - \\ & \frac{\gamma\hat{\phi}(k_i)\phi(k)}{\lambda + \hat{\phi}(k_i)^2}[y_d(k+1) - y(k_i) - \hat{z}_2(k_i)]\end{aligned} \tag{29}$$

where $y_d(k+1) - y(k_i)$ can be processed as

$$\begin{aligned}y_d(k+1) - y(k_i) = & y_d(k+1) - y_d(k) + y_d(k) - \\ & y(k) + y(k) - y(k_i) = \\ & \Delta y_d(k+1) + \tilde{y}(k) + m(k)\end{aligned} \tag{30}$$

Therefore, we obtain

$$\begin{aligned}\tilde{y}(k+1) = \Delta y_d(k+1) + \tilde{y}(k) - \frac{\gamma\hat{\phi}(k_i)\phi(k)}{\lambda + \hat{\phi}(k_i)^2}\cdot \\ [\Delta y_d(k+1) + \tilde{y}(k) + m(k) - \hat{z}_2(k_i)] - \omega(k)\end{aligned} \tag{31}$$

According to the event-triggered condition in Eq. (12), it can be obtained that $g(k) = |h(k)|/\vartheta + \varpi - |m(k)| \geqslant 0$ at $k \in [k_i, k_{i+1})$, that is to say, $|m(k)| \leqslant |h(k)|/\vartheta + \varpi$. Then, applying the absolute value to Eq. (31) gives

$$\begin{aligned}|\tilde{y}(k+1)| \leqslant |\Delta y_d(k+1)| + |\tilde{y}(k)| + \left|1 - \frac{\gamma\hat{\phi}(k_i)\phi(k)}{\lambda + \hat{\phi}(k_i)^2}\right|\cdot \\ |\Delta y_d(k+1) + \tilde{y}(k) + m(k) - \hat{z}_2(k_i)| + |\omega(k)|\end{aligned} \tag{32}$$

where $|\Delta y_d(k+1) + \tilde{y}(k) + m(k) - \hat{z}_2(k_i)| \leqslant |\Delta y_d(k+1)| + |\tilde{y}(k)| +$

$|m(k)|+|\hat{z}_2(k_i)|$. In addition, $\hat{\phi}(k_i)$ and $\hat{z}_2(k_i)$ only update data from $\hat{\phi}(k)$ and $\hat{z}_2(k)$ when dynamic ETM is triggered, and their values will remain unchanged in the other cases. This also means that the boundedness of $\hat{\phi}(k_i)$ and $\hat{z}_2(k_i)$ is consistent with the boundedness of $\hat{\phi}(k)$ and $\hat{z}_2(k)$.

According to $|m(k)| \leqslant |h(k)|/\vartheta + \varpi$, we have

$$\begin{aligned} |\tilde{y}(k+1)| \leqslant & \left|1-\frac{\gamma\hat{\phi}(k_i)\phi(k)}{\lambda+\hat{\phi}(k_i)^2}\right| |\tilde{y}(k)| + \\ & \left|1-\frac{\gamma\hat{\phi}(k_i)\phi(k)}{\lambda+\hat{\phi}(k_i)^2}\right| |\Delta y_d(k+1)| + \\ & \left|\frac{\gamma\hat{\phi}(k_i)\phi(k)}{\lambda+\hat{\phi}(k_i)^2}\right| \left(\frac{1}{\vartheta}|h(k)|+\varpi\right) + \\ & \left|\frac{\gamma\hat{\phi}(k_i)\phi(k)}{\lambda+\hat{\phi}(k_i)^2}\right| |\hat{z}_2(k_i)| + |\omega(k)| \end{aligned} \tag{33}$$

Let $\lambda_{\min} = b_\phi^2/4$, when $\lambda > \lambda_{\min}$, we can find a constant $0 < N < 1$ that makes

$$0 < N < \frac{\hat{\phi}(k_i)\phi(k)}{\lambda+\hat{\phi}(k_i)^2} \leqslant \frac{b_\phi\hat{\phi}(k_i)}{2\sqrt{\lambda}\hat{\phi}(k_i)} < \frac{b_\phi}{2\sqrt{\lambda_{\min}}} = 1 \tag{34}$$

Since $0 < \gamma < 1$, there must be a constant g_2 that

$$\left|1-\frac{\gamma\hat{\phi}(k_i)\phi(k)}{\lambda+\hat{\phi}(k_i)^2}\right| = 1-\frac{\gamma\hat{\phi}(k_i)\phi(k)}{\lambda+\hat{\phi}(k_i)^2} \leqslant 1-\gamma N \overset{\Delta}{=} g_2 < 1 \tag{35}$$

According to Assumption 5 and Theorem 2, we can get $|\Delta y_d(k+1)| \leqslant b_{\Delta,y}$, $|\omega(k)| \leqslant b_\omega$, and $|\hat{z}_2(k_i)| \leqslant b_{\hat{z},2}$, where $b_{\hat{z},2}$ is a constant. Then, combining Formulas (34) and (35), it follows that

$$\begin{aligned} |\tilde{y}(k+1)| \leqslant & g_2|\tilde{y}(k)| + g_2 b_{\Delta,y} + \frac{1}{\vartheta}|h(k)| + \varpi + b_{\hat{z},2} + b_\omega \leqslant \\ & g_2|\tilde{y}(k)| + \Omega(k) \end{aligned} \tag{36}$$

where $\Omega(k) = g_2 b_{\Delta,y} + |h(k)|/\vartheta + \varpi + b_{\hat{z},2} + b_\omega$. The $h(k)$ is bounded by Formula (28), therefore $\Omega(k)$ is also bounded, recorded as $\Omega(k) \leqslant b_\Omega$, where b_Ω is a constant. Then, this yields

$$\begin{aligned} |\tilde{y}(k+1)| \leqslant & g_2|\tilde{y}(k)| + b_\Omega \leqslant \\ & g_2^2|\tilde{y}(k-1)| + g_2 b_\Omega + b_\Omega \leqslant \\ & \cdots \leqslant g_2^k|\tilde{y}(1)| + \frac{b_\Omega(1-g_2^k)}{1-g_2} \end{aligned} \tag{37}$$

When $k \to \infty$, $\dfrac{b_\Omega(1-g_2^k)}{1-g_2} = \dfrac{b_\Omega}{1-g_2}$. This means that $\tilde{y}(k)$ is UUB. ■

Remark 2 As a discrete-time system, the time of Eq. (5) is quantized into minimal indivisible units T_s. The system states are updated exclusively at discrete time instants $k = 0, 1, 2, \ldots$, which can guarantee the absence of Zeno behavior after incorporating the ETM.

IV. Simulation Results

To substantiate the effectiveness of the proposed ESO-based MFAHC strategy, the "Dolphin I" USV [14] is employed for comprehensive simulation analysis, of which model parameters are $K = 0.186$ and $T = 1.068$.

The simulation is conducted in two comparative tests. First, the conventional control scheme without ETM is compared with the approach from Ref. [14]. Subsequently, the proposed control strategy with ETM is compared with the approach from Ref. [22]. The same internal uncertainty and external disturbance are added to two simulation environments at $k \geqslant 200$. Its specific form is

$$K = \begin{cases} 0.186, \ k < 200; \\ 0.186 + 0.02 \cdot \cos\left(\dfrac{k-200}{200} \cdot \pi\right), \ k \geqslant 200 \end{cases} \tag{38}$$

$$d(k) = \begin{cases} 0, \ k < 200; \\ 0.1 \cdot \sin\left(\dfrac{k-200}{400} \cdot 7\pi\right), \ k \geqslant 200 \end{cases} \tag{39}$$

The sampling interval is $T_s = 0.1$ s. The state at $k = 0$ of the heading control system is $r(k) = 0\,°/\mathrm{s}$ and $\psi(0) = 0°$. The parameters of ESO-based MFAHC algorithm are set as $c = 22$, $\eta = 1$, $\mu = 100$, $\varepsilon = 5 \times 10^{-4}$, $\hat{\phi}(0) = 5$, $l_1 = 2$, $l_2 = 1$, $\gamma = 0.35$, $\lambda = 10$, $h_0 = 0$, $\vartheta = 14$, $\varpi = 0.02$, and $\varphi = 0.5$. The desired signals are set to $\psi_d(k) = 45°$ and $r_d(k) = 0\,°/\mathrm{s}$. The other parameters of dynamic event-triggered RO-MFAC (DET-RO-MFAC) [22] and RO-MFAC [14] are the same as the proposed ESO-based MFAHC.

The comparative effects of heading control are shown in Figs. 2 and 3. The differences between the two tests are shown in Table 1. Fig. 4 shows the observed effect of the proposed discrete linear ESO on the lumped disturbance term $\omega(k)$

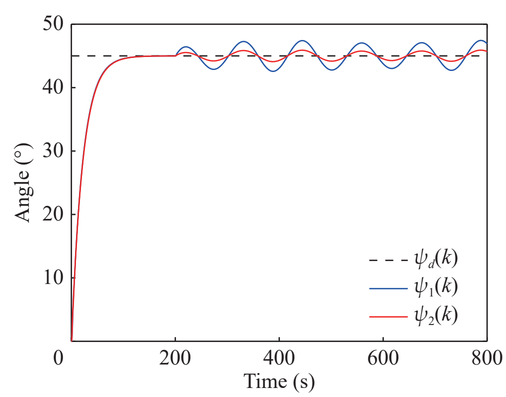

Fig. 2 Comparison result of RO-MFAC and ESO-based MFAHC.

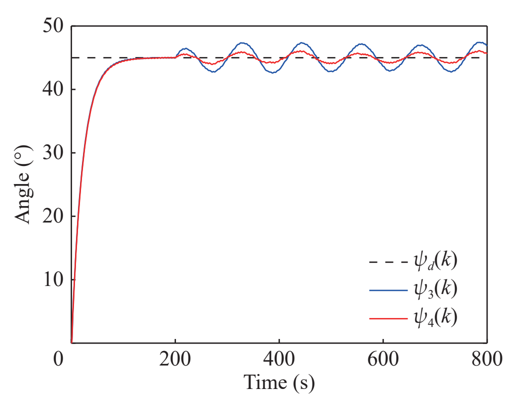

Fig. 3 Comparison result of DET-RO-MFAC and ESO-based MFAHC with dynamic ETM.

without dynamic ETM. Fig. 5 shows the corresponding control input $\delta(k)$ variation curve during this process. Fig. 6 illustrates the triggered intervals of the dynamic ETM for the sensor channel in the heading control system. Compared with

Table 1 Comparison of simulation results.

Control mode	Mark	ESO	ETM	Over shoot
RO-MFAC	$\psi_1(k)$	No	No	2.43°
ESO-based MFAHC¹	$\psi_2(k)$	Yes	No	0.90°
DET-RO-MFAC	$\psi_3(k)$	No	Yes	2.41°
ESO-based MFAHC²	$\psi_4(k)$	Yes	Yes	1.11°

Note: ESO-based MFAHC¹ represents the proposed ESO-based MFAHC without ETM, and ESO-based MFAHC² represents the proposed ESO-based MFAHC with ETM.

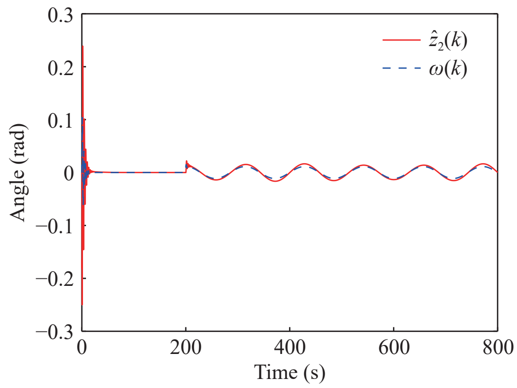

Fig. 4 Estimation effect of ESO-based MFAHC.

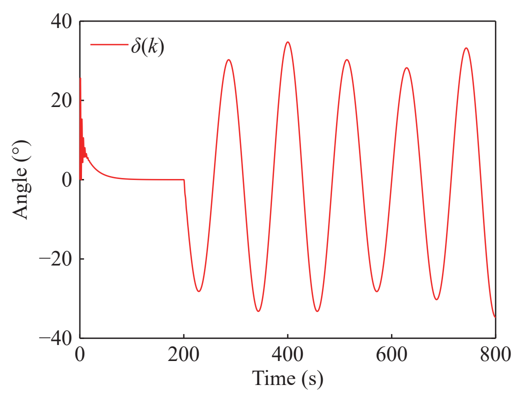

Fig. 5 Rudder angle variation curve of the ESO-based MFAHC.

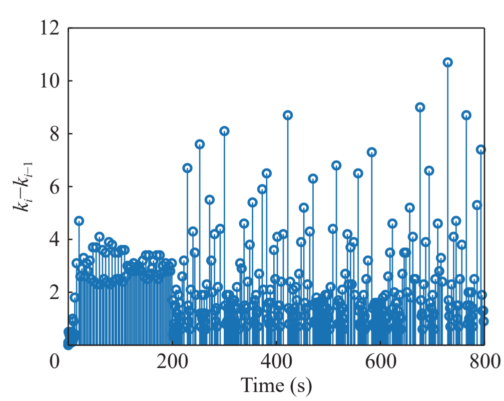

Fig. 6 Event-triggered time interval.

the periodic sampling, the effect of introducing dynamic ETM on saving communication resources is shown in Table 2. The cumulative number of event-triggered occurrences is 428, accounting for 5.35% of the total discrete time intervals of 8000. Fig. 7 shows the observed effect of the proposed discrete linear ESO on the lumped disturbance $\omega(k)$ with the addition of dynamic ETM. Fig. 8 shows the corresponding control input rudder angle variation curve during this process.

Table 2 Effect of dynamic ETM.

Communication mode	Number	Over shoot
Periodic sampling	8000	0.90°
Dynamic ETM	428	1.11°

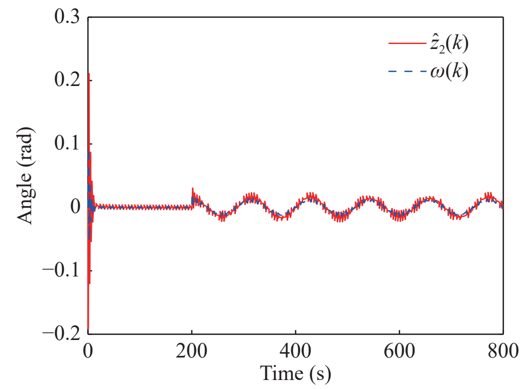

Fig. 7 Estimation effect of ESO-based MFAHC with dynamic ETM.

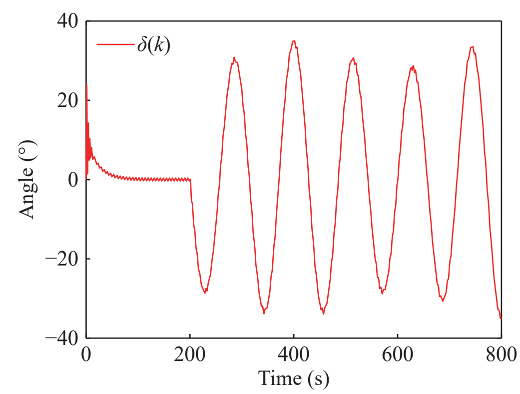

Fig. 8 Rudder angle variation curve of the ESO-based MFAHC with dynamic ETM.

As shown in Table 1 and Figs. 2 and 3, the introduction of discrete linear ESO significantly reduces the oscillation amplitude in heading step response curves. This effect persists regardless of ETM presence, and is particularly pronounced during periods with applied internal model perturbation and external disturbance. This also means that compared with the traditional model-free heading control methods without ESO, the proposed ESO-based MFAHC has better robustness. Figs. 4 and 5 demonstrate that $\hat{z}_2(k)$ can effectively estimate $\omega(k)$. Compensation for this term in the control algorithm ensures the precision and robustness of the proposed heading control strategy under both internal uncertainties and external disturbances. Fig. 6 and Table 2 reveal that the dynamic ETM reduces unnecessary data transmission, thereby conserving limited network resources. Furthermore, Figs. 7 and 8 confirm that both discrete linear ESO and RO-MFAC controllers maintain effective operational status after dynamic ETM adoption. Even with only 5.35% of the communication data, the proposed ESO-based MFAHC with dynamic ETM can still control the heading holding error within an acceptable range. Collectively, the simulation ultimately verifies that the proposed scheme has strong robustness, which achieves reliable heading control performance in simulated marine environments with external disturbances and internal uncertainties.

V. Conclusion

This paper focuses on USV heading control subject to lumped disturbance and non-self-stabilizing characteristics. The proposed MFAHC strategy integrates a discrete linear ESO with MFAC, which can achieve satisfied control effect and economize communication resource without relying on model information. Rigorous derivations demonstrate the bounded stability of the proposed ESO-based MFAHC strategy. Simulation results further confirm that the proposed ESO-based MFAHC approach exhibits superior control performance and effective solution for maritime navigation under challenging conditions. Future work will focus on the experimental validation via a physical USV platform.

Acknowledgment

This work was supported by the Shandong Provincial Natural Science Foundation (Nos. ZR2023QF039 and ZR2024MF068), the Taishan Scholars Project of Shandong Province of China (No. tstp20230624), and the National Natural Science Foundation of China (No. 62373205).

References

[1] T. I. Fossen, *Handbook of Marine Craft Hydrodynamics and Motion Control*. Chichester, UK: Wiley, 2011.

[2] H. Zheng and C. Liu, An overview of unmanned surface vehicles: Metshods, practices, and applications, *Control Eng. Pract.*, 2025, 164, 106479.

[3] Q. Wei, Z. Zhu, J. Zhang, and F.-Y. Wang, A parallel control method for zero-sum game with unknown time-varying system, *Int. J. Intell. Control Syst.,* 2024, 29(1), 37–41.

[4] F. Liu, K. Zhang, Y. Wu, and X. Xue, Interval-constraint multiagent systems: Global attractivity and structural stability of equilibria, *Automatica*, 2026, 183, 112566.

[5] T. I. Fossen, *Marine Control Systems Guidance, Navigation, and Control of Ships, Rigs and Underwater Vehicles*. Trondheim, Norway: Marine Cybernetics, 2002.

[6] S. Li and Y. Liu, Model-free adaptive event-triggered path following control for underactuated autonomous surface vehicles, *Ocean Eng.*, 2025, 341(Pt4), 122725.

[7] J. Du, A. Abraham, S. Yu, and J. Zhao, Adaptive dynamic surface control with Nussbaum gain for course-keeping of ships, *Eng. Appl. Artif. Intell.*, 2014, 27, 236–240.

[8] Z. Peng, D. Wang, W. Wang, and L. Liu, Neural adaptive steering of an unmanned surface vehicle with measurement noises, *Neurocomputing*, 2016, 186, 228–234.

[9] N. Wang, S. Lv, and Z. Liu, Global finite-time heading control of surface vehicles, *Neurocomputing*, 2016, 175, 662–666.

[10] J. Du, X. Hu, and Y. Sun, Adaptive robust nonlinear control design for course tracking of ships subject to external disturbances and input saturation, *IEEE Trans. Syst., Man, Cybern.: Syst.*, 2020, 50(1), 193–202.

[11] Z. Hou and S. Jin, A novel data-driven control approach for a class of discrete-time nonlinear systems, *IEEE Trans. Control Syst. Technol.*, 2011, 19(6), 1549–1558.

[12] Z. Hou and S. Xiong, On model-free adaptive control and its stability analysis, *IEEE Trans. Automat. Control*, 2019, 64(11), 4555–4569.

[13] S. Xiong and Z. Hou, Model-free adaptive control for unknown MIMO nonaffine nonlinear discrete-time systems with experimental validation, *IEEE Trans. Neural Netw. Learn. Syst.*, 2022, 33(4), 1727–1739.

[14] Y. Liao, Q. Jiang, T. Du, and W. Jiang, Redefined output model-free adaptive control method and unmanned surface vehicle heading control, *IEEE J. Oceanic Eng.*, 2020, 45(3), 714–723.

[15] Q. Jiang, Y. Liao, Y. Li, J. Fan, and Y. Miao, Heading control of unmanned surface vehicle with variable output constraint model-free adaptive control algorithm, *IEEE Access*, 2019, 7, 131008–131018.

[16] Y. Liao, C. Chen, T. Du, B. Wang, and Y. Li, Variable output model-free adaptive heading control method for unmanned surface vehicle, *Chin. J. Ship Res.*, 2024, 19(1), 75–83, (in Chinese).

[17] L. Xing, C. Wen, Z. Liu, H. Su, and J. Cai, Event-triggered adaptive control for a class of uncertain nonlinear systems, *IEEE Trans. Automat. Control*, 2017, 62(4), 2071–2076.

[18] T. Zhang, H. Wang, W. Che, and Q. Li, Adaptive event-triggered path following control for networked autonomous vehicles under aperiodic denial-of-service attacks, *J. Control Dec.*, 2024, 11(4), 545–562.

[19] S.-Q. Zhang, W.-W. Che, and C. Deng, Observer-based event-triggered control for linear MASs under a directed graph and DoS attacks, *J. Control Dec.,* 2022, 9(3), 384–396.

[20] Y.-S. Ma, W.-W. Che, and C. Deng, Event-triggered model-free adaptive control for nonlinear cyber-physical systems with false data injection attacks, *Int. J. Robust Nonlinear Control,* 2022, 32(4), 2442–2452.

[21] Y.-S. Ma, W.-W. Che, and C. Deng, Dynamic event-triggered model-free adaptive control for nonlinear CPSs under aperiodic DoS attacks, *Inf. Sci.,* 2022, 589, 790–801.

[22] H. Zhao, D. Xu, Z. Zhou, and H. Yu, Dynamic event-triggered resilient heading control for unmanned surface vehicle with encrypted data, *IEEE Trans. Intell. Veh.*, 2024, 9(9), 5718–5727.

[23] J. Ning, Y. Ma, L. Liu, and T. Li, Fuzzy course tracking control of an unmanned surface vehicle with event-triggered mechanism and input quantization, *Ocean Eng.*, 2023, 288(Pt1), 115704.

[24] B. Van Scoy and L. Lessard, Integral quadratic constraints: Exact convergence rates and worst-case trajectories, in *Proc. 2019 IEEE 58th Conference on Decision and Control*, Nice, France, 2019, 7677–7682.

Shuaixi Li received the BS degree in automation from Qingdao University, Qingdao, China, in 2022. He is currently pursuing the MS degree in systems science at School of Automation, Qingdao University, Qingdao, China. His research interests include guidance and control for unmanned surface vehicles.

Yongchao Liu received the PhD degree in control science and engineering from Harbin Engineering University, Harbin, China, in 2021. He is currently an associate professor at School of Automation, Qingdao University, Qingdao, China. His research interests include adaptive control, data-driven control, and their applications for nonlinear systems.

Ge Song received the PhD degree in control science and engineering from Harbin Engineering University, Harbin, China, in 2022. From 2021 to 2022, she was a visiting student at Institute for Aerospace Studies, University of Toronto, Toronto, Canada. She is currently a lecturer at School of Automation, Harbin University of Science and Technology, China. Her research interests include swarm control of unmanned aerial vehicles, fault-tolerant control, and event-triggered control.